BIT

Fourier spectral methods for fractional-in-space reaction-diffusion equations

**Alfonso Bueno-Orovio · David Kay ·
Kevin Burrage**

Abstract Fractional differential equations are becoming increasingly used as a powerful modelling approach for understanding the many aspects of nonlocality and spatial heterogeneity. However, the numerical approximation of these models is demanding and imposes a number of computational constraints. In this paper, we introduce Fourier spectral methods as an attractive and easy-to-code alternative for the integration of fractional-in-space reaction-diffusion equations described by the fractional Laplacian in bounded rectangular domains of $\mathbb{R}^n$. The main advantages of the proposed schemes is that they yield a fully diagonal representation of the fractional operator, with increased accuracy and efficiency when compared to low-order counterparts, and a completely straightforward extension to two and three spatial dimensions. Our approach is illustrated by solving several problems of practical interest, including the fractional Allen–Cahn, FitzHugh–Nagumo and Gray–Scott models, together with an analysis of the properties of these systems in terms of the fractional power of the underlying Laplacian operator.

A. Bueno-Orovio (✉)
Oxford Centre for Collaborative Applied Mathematics, University of Oxford, Oxford OX1 3LB, UK
e-mail: alfonso.bueno@cs.ox.ac.uk

A. Bueno-Orovio · D. Kay · K. Burrage
Department of Computer Science, University of Oxford, Oxford OX1 3QD, UK

K. Burrage
School of Mathematical Sciences, Queensland University of Technology, Brisbane 4001, Australia

🖄 Springer

1 Introduction

Fractional differential equations are becoming increasingly used as a modelling tool for
diffusive processes associated with sub-diffusion (fractional in time), super-diffusion
(fractional in space) or both, and have a long history in, for example, physics, finance,
mathematical biology and hydrology. In water resources, fractional models have been
used to describe chemical and pollute transport in heterogeneous aquifers [1,5,28].
In finance, they have been used because of the relationship with certain option pric-
ing mechanisms and heavy tailed stochastic processes [37]. More recently, fractional
models of the Bloch–Torrey equation have been used in magnetic resonance [27].

In this paper we will only consider super-diffusion effects (space-fractional mod-
els) in spatially extended structures. In this context, random walks (and the asso-
ciated standard diffusion equation) may have limitations, and they do not apply to
cases where extended heterogeneities or spatial connectivities of the medium can
facilitate transport processes within certain space scales, which can be interpreted as
temporal correlations on all time scales [45]. These inhomogeneities of the medium
may fundamentally alter the laws of Markov diffusion, leading to long range fluxes,
and non-Gaussian, heavy tailed profiles [4,30]. Different generalizations of Brownian
motion have been developed to describe these situations, as Lévy walks, where parti-
cles dynamics are sampled from a probabilistic distribution that decays as a power law
instead of exponential decay. In the continuous limit, the analogy between Lévy flights
and certain types of space-fractional models has been established [30]. As such, these
fractional models can be viewed as describing the probability time-space distribution
of an ensemble of particles undergoing stochastic Lévy walks, with a heavy tailed
distribution characteristic of anomalous diffusion.

A standard approach for solving fractional in space diffusion problems is to apply a
finite difference, finite element or finite volume discretisation of the fractional operator,
and then use a semi-implicit Euler formulation for the time evolution of the solution.
This requires the solution of a linear system of equations at each time step, whose left
hand side matrix has a fractional power. The main hurdle to overcome is the non-local
nature of the fractional operator, which leads to large, dense matrices. Various authors
such as Ilić et al. [18], Meerschaert et al. [29], Roop [35], Wang et al. [40,41], Liu
et al. [25] and Pang et al. [33] have considered the numerical solution of such problems
using various discretisations, but most of these approaches either do not scale well or
their scalability has not been demonstrated. Even the construction of such matrices
presents difficulties, especially in efficiency [35]. Very recently, two approaches have
been developed that use Krylov approaches [43] or fast numerical integration in con-
junction with effective preconditioners and matrix transfer techniques [11] that allow
for problems in two or three spatial dimensions to be tackled. However, even these
latter approaches do not scale perfectly as the spatial dimension increases to three and

their effectiveness still depends on the mesh discretisation. Alternatively, in the setting of a Riesz fractional derivative formulation, a finite difference formula on tensor grids using a shifted Grünwald discretisation may be applied, which leads to relatively sparse, well structured, positive definite matrices [18,25,29,42]. The solution of these linear systems can be approximated efficiently using a combination of multigrid and conjugate gradient methods [33].

Despite their higher order of convergence when compared to low order stencils and being in nature nonlocal, little use has been made of spectral methods for the solution of fractional-in-space equations. Li and Xu [24] have considered a spectral approach for the weak solution of the space-time fractional diffusion equation. Khader et al. [20,21]have proposed Chebyshev and Legendre Galerkin methods for the discretisation of fractional advection-dispersion equations where the spatial derivatives are considered in the Caputo sense, similar to the results of Li and Xu [23] for the time-fractional diffusion equation. Hanert [17] also has considered the use of a Chebyshev spectral element method for the numerical solution of the fractional Riemann–Louiville advection-diffusion equation for tracer transport. Very recently, a collocation method based on fractional Lagrange interpolants has been presented by Zayernouri and Karniadakis [44] for solving steady-state and time-dependent fractional partial differential equations. However, all previous works were restricted to one-dimensional simulations, and to our knowledge there is no rigorous study on the application of Fourier spectral methods to fractional-in-space reaction-diffusion equations. This will be the main contribution of this paper, where we introduce Fourier spectral methods as an efficient alternative approach to solving fractional reaction-diffusion problems in rectangular domains of $\mathbb{R}^n$. The main advantage of this approach is that it gives a full diagonal representation of the fractional operator, being able to achieve spectral convergence regardless of the fractional power in the problem. An additional advantage is that the application to two and three spatial dimensions is essentially the same as the one dimensional problem.

The outline of the paper is as follows. Section 2 gives the main elements of our spectral approach and presents convergence results for different types of initial and boundary conditions. In Sect. 3 we present the applicability of these ideas to a number of important problems in mathematical modelling: (1) the Allen–Cahn equation, which describes domain coarsening kinetics in alloys and other systems developing formation and motion of phase boundaries [3,11]; (2) the FitzHugh–Nagumo model, as a model to represent impulse propagation in nerve membranes [14,32], and the basis for more sophisticated models of cardiac electrophysiology [8]; and (3) the Gray-Scott model [15,16], as an example of autocatalytic chemical reaction with important applications to the study of pattern formation and morphogenesis [22,34]. Finally, Sect. 4 offers some conclusions and thoughts for future work.

2 Fourier spectral method for fractional diffusion

A space fractional diffusion equation can be derived by replacing the standard Laplace operator by its fractional counterpart

$$\partial_t u = -K(-\Delta)^{\alpha/2}u, \quad 0 < \alpha \leq 2, \quad \mathbf{x} \in \Omega \subset \mathbb{R}^n, \tag{2.1}$$

with initial condition $u(\mathbf{x}, 0) = u_0(\mathbf{x}) \in L^2(\Omega)$, where K is the conductivity or diffusion coefficient and $(-\Delta)^{\alpha/2}$ is the fractional Laplacian [18,39,42]. The system is closed with either a homogeneous Dirichlet boundary condition, representing a fixed concentration of u on $\partial\Omega$, or a homogeneous Neumann one, where mass is conserved in Ω [18].

Spectral decomposition plays a central role in the interpretation of the fractional Laplacian – see [18] and [42]. Suppose the Laplacian $(-\Delta)$ has a complete set of orthonormal eigenfunctions $\{\varphi_j\}$ satisfying standard boundary conditions on a bounded region $\Omega \subset \mathbb{R}^n$, with corresponding eigenvalues λ_j, i.e., $(-\Delta)\varphi_j = \lambda_j\varphi_j$ on Ω, and let

$$\mathcal{U}_\alpha := \left\{ u = \sum_{j=0}^{\infty} \hat{u}_j \varphi_j, \;\; \hat{u}_j = \langle u, \varphi_j \rangle, \;\; \sum_{j=0}^{\infty} |\hat{u}_j|^2 |\lambda_j|^{\alpha/2} < \infty, \;\; 0 < \alpha \le 2 \right\}. \tag{2.2}$$

Then, for any $u \in \mathcal{U}_\alpha$,

$$(-\Delta)^{\alpha/2} u = \sum_{j=0}^{\infty} \hat{u}_j \lambda_j^{\alpha/2} \varphi_j. \tag{2.3}$$

Therefore, $(-\Delta)^{\alpha/2}$ has the same interpretation as $(-\Delta)$ in terms of its spectral decomposition. Furthermore, the former result suggests that a spectral approach may be feasible for solving problems in the form of (2.1). In fact, the spectral decomposition given by Eqs. (2.2)–(2.3) is well known, and has been previously used in combination with trigonometric (Fourier) basis functions to obtain analytical benchmark solutions for problems in the form of (2.1) [19,42,43]. However, its use has been restricted to situations where the integrals defining the Fourier coefficients $\hat{u}_j$ of the associated initial data can be calculated in closed form. Here we show how to develop suitable numerical methods allowing for a straightforward use of (2.2)–(2.3) without such explicit calculations, and, in particular, their extension for the solution of nonlinear reaction-diffusion systems governed by the fractional Laplacian.

2.1 Space discretisation

In order to present the basis of the method, let us consider for simplicity the fractional heat Eq. (2.1) in one space dimension, subject to $u(x, 0) = u_0(x)$ and homogeneous Dirichlet or Neumann boundary conditions in $x \in [a, b]$. By using (2.2)–(2.3), we can easily derive the analytical solution of (2.1) as

$$u(x, t) = \sum_{j=0}^{\infty} \hat{u}_j(t)\varphi_j(x) = \sum_{j=0}^{\infty} \hat{u}_j(0)e^{-K\lambda_j^{\alpha/2}t} \varphi_j(x), \tag{2.4}$$

with $\hat{u}_j(0) = \langle u_0(x), \varphi_j(x) \rangle$. Eigenfunctions and eigenvalues will depend on the specified boundary conditions: $\lambda_j = \left(\frac{(j+1)\pi}{L}\right)^2$, $\varphi_j = \sqrt{\frac{2}{L}} \sin\left(\frac{(j+1)\pi(x-a)}{L}\right)$ for

homogeneous Dirichlet, or $\lambda_j = \left(\frac{j\pi}{L}\right)^2$, $\varphi_j = \sqrt{\frac{2}{L}} \cos\left(\frac{j\pi(x-a)}{L}\right)$ for the homogeneous Neumann type, where $L = b - a$.

Fourier spectral methods represent the truncated series expansion of (2.4) when a finite number of orthonormal trigonometric eigenfunctions $\{\varphi_j\}$ (equal to the number of discretisation points) are considered

$$u(x,t) \approx \sum_{j=0}^{N-1} \hat{u}_j(t)\varphi_j(x) = \sum_{j=0}^{N-1} \hat{u}_j(0)e^{-K\lambda_j^{\alpha/2}t}\varphi_j(x). \qquad (2.5)$$

For each of the specified types of boundary data, coefficients $\hat{u}_j$ in (2.5), as well as the inverse reconstruction of u in physical space, can be efficiently computed by fast and robust existing algorithms (direct and inverse Discrete Sine/Cosine Transforms, see [6,9]). To illustrate the ease of application of the approach, the 5-lines of MATLAB Codes 1 and 2 exemplify the numerical solution of (2.1) in $x \in [-L/2, L/2]$, subject to homogeneous Dirichlet and Neumann boundary conditions, respectively. In all the codes provided, N represents the number of internal equispaced mesh points, hence not including boundary nodes. These restrictions in mesh generation are implicitly requested by the respective discrete transforms, so that the extension of the numerical solution avoids repetition of boundary values, therefore keeping C^∞ at the discrete level [6]. The above conditions can be easily accommodated by the choice of meshes given by

$$\text{Dirichlet}: \qquad x_n = a + n\Delta x, \qquad \Delta x = L/(N+1),$$
$$\text{Neumann}: \quad x_n = a + (n-1)\Delta x + \Delta x/2, \quad \Delta x = L/N,$$

where $n \in \{1, N\}$. For the same number of internal discretisation points N, the corresponding Δx in both cases is clearly illustrated by Fig. 1.

Code 1 Fractional heat equation (homogeneous Dirichlet boundary conditions). `dst/idst` are the direct/inverse MATLAB implementations of the Discrete Sine Transform.

```
1  function u = fractional_heat_dirichlet(L,N,K,alpha,t)
2  lambda = (((1:N)*pi/L).^2).^(alpha/2);        % Eigenvalues
3  dx = L/(N+1); x = -L/2+(1:N)*dx;              % Mesh generation
4  k = 25; u = exp(-k*x.^2./(1-x.^2));           % Initial condition
5  u = idst(exp(-K*lambda*t).*dst(u));           % Spectral solution
```

Code 2 Fractional heat equation (homogeneous Neumann boundary conditions). `dct/idct` are the direct/inverse MATLAB implementations of the Discrete Cosine Transform.

```
1  function u = fractional_heat_neumann(L,N,K,alpha,t)
2  lambda = (((0:N-1)*pi/L).^2).^(alpha/2);      % Eigenvalues
3  dx = L/N; x = -L/2+(0:N-1)*dx+dx/2;           % Mesh generation
4  k = 25; u = tanh(k*x./sqrt(1-x.^2));          % Initial condition
5  u = idct(exp(-K*lambda*t).*dct(u));           % Spectral solution
```
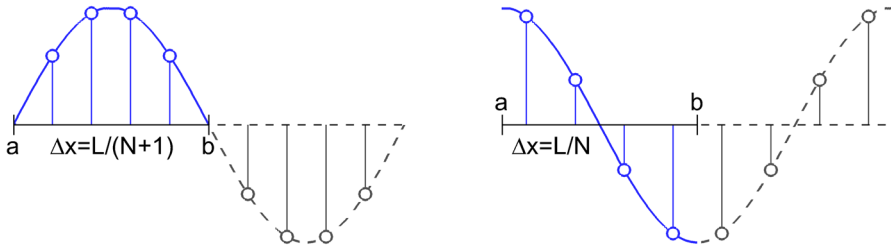
Fig. 1 Selection of appropriate internal nodes for mesh discretisation for homogeneous Dirichlet (*left*) and homogeneous Neumann (*right*) boundary conditions, in order to ensure continuity of the periodic extension of the solutions at the discrete level (*dashed lines*)
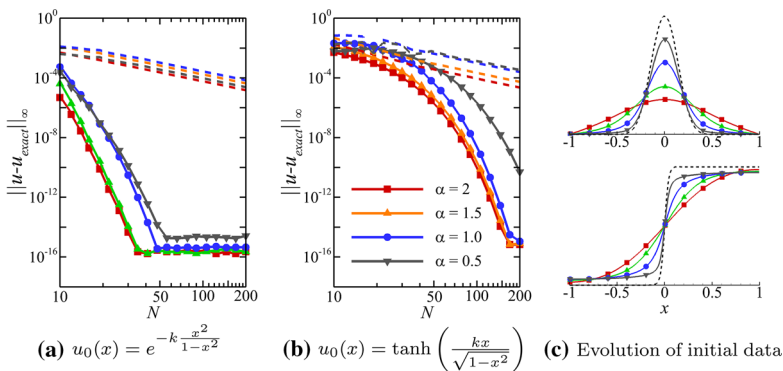
2.2 Convergence in space

Equivalently, the solution of (2.1) using a finite differences or finite elements matrix-based approach can be approximated as

$$\mathbf{u}(t) \approx \mathbf{Q} \, diag \left\{ e^{-K\lambda_0^{\alpha/2}t}, e^{-K\lambda_1^{\alpha/2}t}, \dots, e^{-K\lambda_{N-1}^{\alpha/2}t} \right\} \mathbf{Q}^{-1}\mathbf{u}_0, \qquad (2.6)$$

where $\mathbf{Q}$ represents the matrix of corresponding eigenvectors and $\mathbf{u}$ denotes the vector of node values of u [43]. Since both (2.5) and (2.6) are exact in time, all of the error in both schemes is associated with the spatial discretisation, so we can use this simple example to study the convergence of the two schemes in the numerical approximation of (2.1) for varying values of the fractional power α.

Convergence results in the ℓ^∞-norm are presented in Fig. 2 for the Fourier and finite differences approximations of (2.1) in $x \in [-1, 1]$ at $t = 0.1$, with $K = 1$. Two different initial conditions were considered: a smooth Gaussian profile, subject to homogeneous Dirichlet conditions (Fig. 2a); and a sigmoid exhibiting sharper gradients, with homogeneous Neumann data (Fig. 2b). Reference solutions were calculated by evaluating (2.4) with 2^{12} Fourier modes, with coefficients $\hat{u}_j$ computed by adaptive Gauss-Kronrod quadrature. In both situations, the Fourier approach is able to achieve

(a) $u_0(x) = e^{-k\frac{x^2}{1-x^2}}$ **(b)** $u_0(x) = \tanh\left(\frac{kx}{\sqrt{1-x^2}}\right)$ **(c)** Evolution of initial data

Fig. 2 Convergence results for the fractional heat equation in one space dimension for Fourier (*solid lines*) and finite differences (*dashed lines*) methods. A value of $k = 25$ was used in both cases. *Right panel* illustrates evolution of initial data (*dashed black lines*) at $t = 0.1$, for $K = 1$ and varying α

spectral convergence up to machine precision regardless of α, whereas the finite differences solutions show the standard $\mathcal{O}(N^{-2})$ accuracy of these schemes. Figure 2c shows the effect of the fractional order in space for this problem, reflecting the slower rate of diffusion for $\alpha < 2$.

The applicability of the spectral approach to higher dimensions is illustrated in Fig. 3 for the numerical solution of the fractional heat equation in $[0, 1]^2$, for different values of the fractional power α and $K = 1$. Fourier and finite difference approximations were computed at $t = 0.1$ (Fig. 3a), subject to homogeneous Dirichlet boundary conditions and initial data $u_0(x, y) = \delta \left(x - \frac{1}{2}, y - \frac{1}{2} \right)$, where $\delta(x, y)$ is the Dirac delta function. Numerical solutions were compared with the analytical solution given in [43] (same choice of α's to facilitate visual comparison), resulting in the convergence plot presented in Fig. 3b, which further evidences the increased accuracy of the spectral approach when compared to lower order counterparts. The associated 7-lines of MATLAB Code 3 also demonstrates the ease of extension of the spectral scheme to higher dimensions, where the multi-dimensional direct/inverse transforms can by easily computed by recursively applying the one-dimensional discrete transformations to each of the spatial dimensions of the data.

Code 3 Fractional heat equation in 2D (homogeneous Dirichlet boundary conditions). Two-dimensional MATLAB implementations of the direct/inverse Discrete Sine Transform (dst2/idst2) are given for completeness.

```
1   function u = fractional_heat_dirichlet_2D (L,N,K, alpha , t )
2   [kx , ky] = meshgrid ((1:N)* pi /L);           % 1D wavenumbers
3   lambda = (kx.^2+ky.^2).^( alpha /2);           % 2D eigenvalues
4   dx = L/(N+1); [X,Y] = meshgrid ((1:Nx)*d );           % Mesh
5   mp = (N−1)/2+1;           % Mid−point of the domain (N odd)
6   u = zeros (N); u(mp,mp) = 1/(dx*dx);           % Initial condition
7   u = idst2 (exp(−K*lambda*t ).* dst2 (u));           % Spectral solution
8
9   function uhat = dst2 (u)
10  uhat = dst ( dst (u).').';           % 2D Discrete Sine Transform
11
12  function u = idst2 (uhat)
13  u = idst ( idst (uhat).').';           % 2D Inverse Sine Transform
```
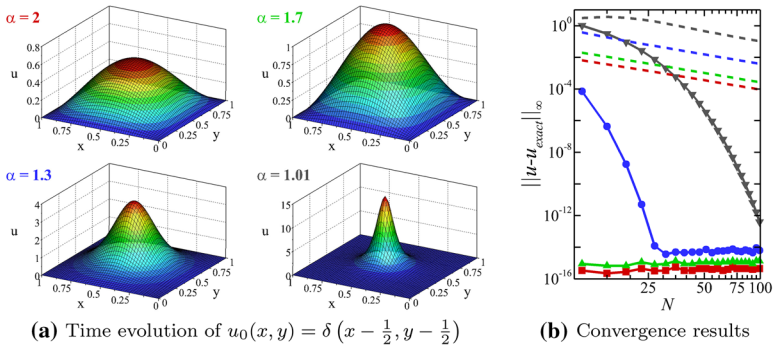
Execution times are given in Tables 1 and 2 for comparison between both methods, showing a much better performance of the Fourier stencil, especially for larger N and higher space dimensions. All computations presented in this work were performed on a standard i5 Intel 2.3 GHz laptop in MATLAB 7.6.

2.3 Time discretisation

For reaction-diffusion systems of P species $\mathbf{u} = [u_1, \ldots, u_P]^T$ in the form of

$$\partial_t u_i = -K_i(-\Delta)^{\alpha/2} u_i + f_i(\mathbf{u}, t), \quad 0 < \alpha \leq 2, \quad \mathbf{x} \in \Omega \subset \mathbb{R}^n, \qquad (2.7)$$

(a) Time evolution of $u_0(x,y) = \delta \left(x - \frac{1}{2}, y - \frac{1}{2}\right)$ **(b)** Convergence results

Fig. 3 Numerical solutions of the fractional heat equation in two space dimensions at $t = 0.1$, for $K = 1$ and varying α. The right panel illustrates convergence results for the Fourier method (*solid lines*) compared to finite differences (*dashed lines*). N indicates the number of discretisation points in each domain direction

Table 1 Timing results (seconds) for solving Eq. (2.1) in one space dimension for different discretisations

N	32	64	128	256	512
Fourier	1.4149e−4	1.7433e−4	2.2572e−4	2.8651e−4	3.8439e−4
Finite differences	6.3810e−4	2.1640e−3	9.4125e−3	5.7550e−2	3.8384e−1

Results are independent of α

Table 2 Timing results (seconds) for solving Eq. (2.1) in two space dimensions for different discretisations

N	19	39	59	79	99
Fourier	5.3956e−4	1.0141e−3	1.8745e−3	2.6891e−3	4.3763e−3
Finite differences	1.2374e−1	8.2588	94.8947	539.7145	2352.0046

N indicates points in each domain direction. Results are independent on α

where K_i is the diffusion coefficient of the ith species u_i and f_i represents its associated reaction term, we consider a backward Euler discretisation of the time derivative presented in [11], where in each time step $[t_n, t_{n+1}]$ the nonlinear term is treated using the following fixed point iteration: given $\mathbf{u}^n$, define $\mathbf{u}^{n+1,0} := \mathbf{u}^n$, and for $m = 1, 2, \ldots, M$ find $\mathbf{u}^{n+1,m}$ such that

$$\frac{u_i^{n+1,m} - u_i^n}{\Delta t} = -K_i(-\Delta)^{\alpha/2} u_i^{n+1,m} + f_i\left(\mathbf{u}^{n+1,m-1}, t^{n+1}\right), \qquad (2.8)$$

where M is to be chosen. Clearly, $M = 1$ leads to the fully explicit treatment of the nonlinear term, and for sufficiently large M the method is fully implicit.

By applying the Fourier transform to both sides of (2.8) and the definition of the fractional Laplacian given by (2.3), one gets

$$\frac{\widehat{u_i}_j^{n+1,m} - \widehat{u_i}_j^n}{\Delta t} = -K_i \lambda_j^{\alpha/2} \widehat{u_i}_j^{n+1,m} + \widehat{f_i}_j\left(\mathbf{u}^{n+1,m-1}, t^{n+1}\right), \qquad (2.9)$$

where $\widehat{f_i}_j$ is the jth Fourier coefficient of the ith reaction term, and the orthogonality of the basis functions has been used, implying that each of the Fourier coefficients

evolves independently to the others. After rearrangement of terms, the time-space discretisation for the jth Fourier mode simply becomes

$$\widehat{u}_{ij}^{n+1,m} = \frac{1}{1 + K_i \lambda_j^{\alpha/2} \Delta t} \left[\widehat{u}_{ij}^n + \Delta t \, \widehat{f}_{ij} \left(\mathbf{u}^{n+1,m-1}, t^{n+1} \right) \right]. \qquad (2.10)$$

Note that (2.10) is fully diagonal, thus requiring no preconditioning, and that it also avoids associated numerical challenges for the treatment of singular Laplacians (containing the eigenvalue $\lambda_j = 0$), as in the case of homogeneous Neumann boundary conditions [11]. Also note that, if any $K_i = 0$, the above stencil simply reduces to the backward Euler discretisation of the given species.

An additional advantage of the proposed time-space stencil is the fully implicit treatment of the fractional Laplacian, resulting in an unconditionally stable scheme in terms of the non-local operator. This can be verified in (2.10) in the absence of reaction sources, since for $f_i(\mathbf{u}, t) = 0$ all Fourier coefficients monotonically decay to zero as $t \to \infty$ (with the exception of the zero-frequency mode associated to $\lambda_j = 0$ in the case of homogeneous Neumann boundary conditions, which remains constant). Any possible time step restrictions will therefore be related only to the explicit treatment of source terms. Hence, the convergence of the proposed fixed point iteration is dependent upon the time step, although in practice, even when using reasonably large time steps, convergence was always experienced. Alternative linearisations of these terms and adapted time stepping may be constructed to improve both the time step restriction and the convergence rates of the ones presented; this constitutes ongoing research.

Code 4 Fractional heat equation in 2D with source term (homogeneous Dirichlet boundary conditions). Two-dimensional Sine Transforms (`dst2/idst2`) as indicated in Code 3.

```
1   function u = fractional_source_2D (L,N,K, alpha , tend , dt ,M)
2   [kx,ky] = meshgrid ((1:N)*pi/L);            % 1D wavenumbers
3   lambda = (kx.^2+ky.^2).^(alpha/2);          % 2D eigenvalues
4   dx = L/(N+1); [X,Y] = meshgrid ((1:N)*dx);      % Mesh
5   v1 =    9*sin(pi*X).*sin(pi*Y);      l1 =   2*pi^2;
6   v2 = -3*sin(pi*X).*sin(3*pi*Y);      l2 = 10*pi^2;
7   v3 = -3*sin(3*pi*X).*sin(pi*Y);      l3 = 10*pi^2;
8   v4 =      sin(3*pi*X).*sin(3*pi*Y);  l4 = 18*pi^2;
9   f1 = K/16*((1+l1^(alpha/2))*v1+(1+l2^(alpha/2))*v2+...
10               (1+l3^(alpha/2))*v3+(1+l4^(alpha/2))*v4);
11  f2 = alpha*sin(pi*X).^3.*sin(pi*Y).^3;        % Source term
12  u = zeros(N);                  % Initial condition
13  for n = 1:round(tend/dt)             % Time-space evolution
14      u0dst = dst2(u); t = n*dt;
15      for m = 1:M               % Fixed-point iteration
16          f = f1*t^alpha + f2*t^(alpha-1) - K*u;
17          u = idst2((u0dst+dt*dst2(f))./(1+K*dt*lambda));
18      end
19  end
```

2.4 Convergence in time

The MATLAB Code 4 exemplifies the use of the above presented time-space stencil (2.10) for the numerical solution of the fractional reaction-diffusion Eq. (2.7) in two space dimensions $(x, y) \in [0, 1]^2$, with

$$f(u, t) = t^\alpha \frac{K}{16} \sum_{i=1}^{4} (1 + \lambda_i^{\alpha/2}) v_i + \alpha t^{\alpha-1} \sin^3(\pi x) \sin^3(\pi y) - Ku \quad (2.11)$$

where
$$
\begin{aligned}
v_1 &= 9 \sin(\pi x) \sin(\pi y), & \lambda_1 &= \pi^2 + \pi^2 \\
v_2 &= -3 \sin(\pi x) \sin(3\pi y), & \lambda_2 &= \pi^2 + (3\pi)^2 \\
v_3 &= -3 \sin(3\pi x) \sin(\pi y), & \lambda_3 &= (3\pi)^2 + \pi^2 \\
v_4 &= \sin(3\pi x) \sin(3\pi y), & \lambda_4 &= (3\pi)^2 + (3\pi)^2,
\end{aligned}
$$

subject to $u(x, y, 0) = 0$ and homogeneous Dirichlet boundary conditions. The exact solution to this problem is $u(x, y, t) = t^\alpha \sin^3(\pi x) \sin^3(\pi y)$, which can be verified by applying Fourier decomposition and Definition (2.3). Errors in the ℓ^∞-norm in the numerical solution at $t = 1$ are listed in Table 3 for different time steps and number of fixed-point iterations, using $\alpha = 1.5$, $K = 10$ and $N = 51$ points in each domain direction. As expected for the implicit Euler method, the order of convergence for the scheme in time is $\mathcal{O}(\Delta t)$. Table 3 also indicates that the numerical error of the method is controlled to a larger extent by the time resolution, Δt, than by the number of fixed-point iterations, M.

3 Fractional-in-space reaction-diffusion systems

The former results show that the global interpolant properties and the diagonal structure of the proposed Fourier spectral method enable the accurate and efficient simulation of fractional-in-space dynamical systems. In this section, we present numerical results of large-scale simulations of different reaction-diffusion models of general interest. Due to their wide use in this type of models, we will concentrate here on the use of homogeneous Neumann boundary conditions, $\partial_n u = 0$. We also restrict our interest to the upper part of the super-diffusive range ($1 < \alpha < 2$), comparing our results against the pure diffusion case ($\alpha = 2$).

Table 3 Time convergence in the solution of the fractional heat Eq. (2.7) in two space dimensions with source term given by (2.11) at $t = 1$ ($\alpha = 1.5$, $N = 51$, $K = 10$), subject to $u(x, y, 0) = 0$ and homogeneous Dirichlet boundary conditions

Δt	0.1	0.05	0.025	1e−3	5e−4	2.5e−4
$M = 1$	1.0070e−2	5.0880e−3	2.5571e−3	1.0279e−4	5.1398e−5	2.5700e−5
$M = 3$	3.3956e−4	1.6201e−4	7.5956e−5	2.5366e−6	1.2653e−6	6.3223e−7
$M = 5$	2.5809e−4	1.2778e−4	6.3547e−5	2.5287e−6	1.2642e−6	6.3208e−7

3.1 Allen–Cahn equation: metastability

The Allen–Cahn equation with a quartic double well potential is a simple nonlinear reaction-diffusion model that arises in the study of formation and motion of phase boundaries. The fractional-in-space version of this equation takes the form

$$\partial_t u = -K(-\Delta)^{\alpha/2}u + u - u^3, \tag{3.1}$$

where K is a small positive constant. The steady states $u = \pm 1$ are attracting, and solutions tend to exhibit flat areas around these two values separated by interfaces of increasing sharpness as the control parameter K is reduced to zero. On the other hand, the state $u = 0$ is unstable, and solutions around this value vanish or coalesce over long time scales in a phenomenon known as metastability [38].

The interfacial properties of the Allen–Cahn equation in the fractional case have been previously analysed [11], indicating that for decreasing α the solution changes significantly faster near the center of the interface. Away from the centre the solutions become less steep and the whole interface becomes thicker, reflecting the non-local character of the fractional operator. However, the effect of fractional diffusion on the metastability of the solutions has still not been studied.

Figure 4 shows the effect of varying α in the metastability of solutions of the Allen–Cahn equation in $x \in [-1, 1]$, with parameter $K = 0.01$ and initial data $u(x, 0) = \frac{1}{2} \sin(\frac{3\pi}{2}x)(\cos(\pi x) - 1)$. For the pure diffusion case (Fig. 4a), the initial data evolves to an intermediate unstable equilibrium, followed by a rapid transition to a solution with just one interface. As the fractional power is decreased, the lifetime of the unstable interface is largely prolonged (Fig. 4b), eventually becoming fully stabilised due to the long-tailed influence of the fractional diffusion process (Fig. 4c). Our last MATLAB example, Code 5, illustrates the solution of the fractional-in-space Allen–Cahn equation using the proposed Fourier method.

Code 5 Fractional Allen–Cahn equation (homogeneous Neumann boundary conditions). `dct/idct` stand for the direct/inverse MATLAB implementations of the Discrete Cosine Transform.

```
1   function u = fractional_allen_cahn (L,N,K,alpha ,tend ,dt ,M)
2   lambda = (((0:N−1)*pi/L).^2).^(alpha/2);        % Eigenvalues
3   dx = L/N;  x = −L/2+(0:N−1)*dx+dx/2;             % Mesh generation
4   u = 0.5*sin(3*pi/2*x).*(cos(pi*x)−1);    % Initial condition
5   for n = 1:round(tend/dt)                  % Time−space evolution
6       u0dct = dct(u);
7       for m = 1:M                           % Fixed−point iteration
8           f = u − u.^3;
9           u = idct((u0dct+dt*dct(f))./(1+K*dt*lambda));
10      end
11  end
```

(a) $\alpha = 2$ **(b)** $\alpha = 1.3$ **(c)** $\alpha = 1.01$
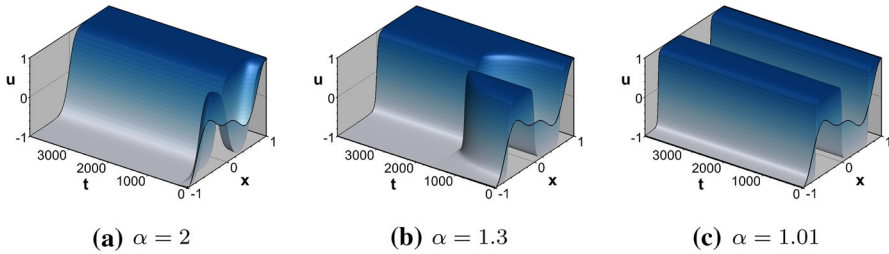
**Fig. 4** Metastability of solutions of the Allen–Cahn equation for varying α

3.2 FitzHugh–Nagumo model: excitable media

The FitzHugh–Nagumo model represents one of the simplest models for the study of excitable media [14,32]. The propagation of the transmembrane potential in the nerve axon is modeled by a diffusion equation with a cubic non-linear reaction term, whereas the recovery of the slow variable is represented by a single ordinary differential equation in the form

$$
\begin{aligned}
\partial_t u &= -K_u(-\Delta)^{\alpha/2} u + u(1-u)(u-a) - v \\
\partial_t v &= \epsilon(\beta u - \gamma v - \delta),
\end{aligned}
\tag{3.2}
$$

where we consider the following choice of model parameters, $a = 0.1$, $\epsilon = 0.01$, $\beta = 0.5$, $\gamma = 1$, $\delta = 0$, which is known to generate stable patterns in the system in the form of re-entrant spiral waves. In our simulations, the trivial state $(u, v) = (0, 0)$ was perturbed by setting the lower-left quarter of the domain to $u = 1$ and the upper half part to $v = 0.1$, which allows the initial condition to curve and rotate clockwise generating the spiral pattern. The domain is taken to be $[0, 2.5]^2$, discretised using $N = 256$ points in each spatial coordinate, with a diffusion coefficient $K_u = 10^{-4}$.

Stable rotating solutions at $t = 2,000$ are presented in Fig. 5 to illustrate the effect of fractional diffusion in the FitzHugh–Nagumo model. The width of the excitation wavefront (red areas) is markedly reduced for decreasing α, so is the wavelength of the system, with the domain being able to accommodate a larger number of wavefronts for smaller α.

(a) $\alpha = 2$ **(b)** $\alpha = 1.7$ **(c)** $\alpha = 1.5$
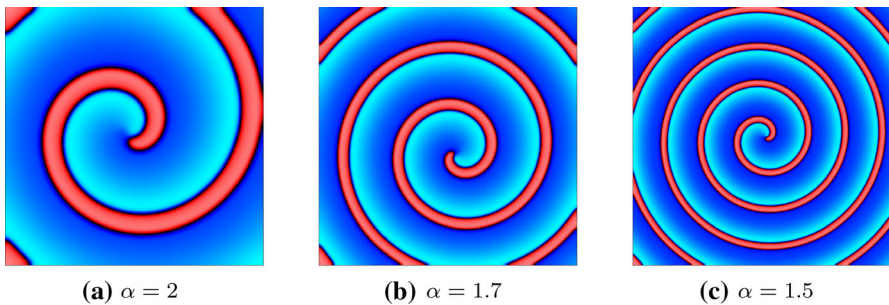
Fig. 5 Spiral waves in the FitzHugh–Nagumo model for varying α

(a) $K_u = 5 \times 10^{-5}$ **(b)** $K_u = 3 \times 10^{-5}$ **(c)** $K_u = 10^{-5}$
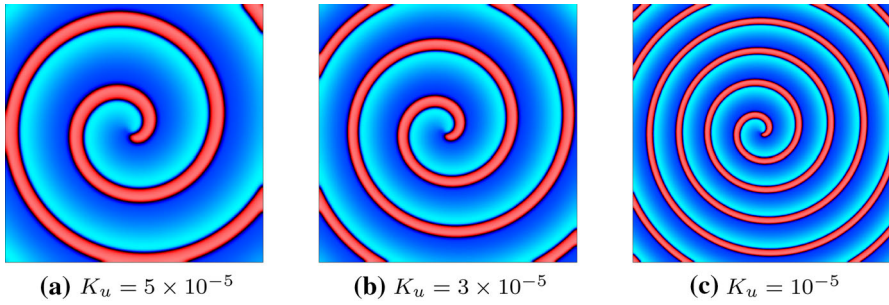
Fig. 6 Solutions of the FitzHugh–Nagumo model for varying diffusion coefficient and $\alpha = 2$

However, it is important to emphasise here that the role of reducing the fractional power α is not equivalent to the influence of a decreased diffusion coefficient in the pure diffusion case (Fig. 6). This can be clearly observed by comparison of Figs. 5b, c and 6b, c: for approximately the same width of the excitation wavefront, the wavelength of the system is larger in the fractional diffusion case, due to the long-tailed mechanisms of the fractional Laplacian operator. These results are therefore consistent with those of Engler [12] for the fractional reaction-diffusion Fisher equation, showing distinct effects of fractional diffusion to those of reduced conductivity for a family of travelling wave solutions. They also illustrate the use of fractional diffusion as a modelling tool to characterise intermediate dynamic states not solely described by pure diffusion mechanisms.

3.3 Gray–Scott model: morphogenesis

The extension of the Fourier stencil to systems of reaction-diffusion equations is as well straightforward. We consider the fractional version of the Gray–Scott model [15,16]

$$\begin{aligned}
\partial_t u &= -K_u(-\Delta)^{\alpha/2}u - uv^2 + F(1-u) \\
\partial_t v &= -K_v(-\Delta)^{\alpha/2}v + uv^2 - (F+\kappa)v,
\end{aligned} \tag{3.3}$$

where K_u, K_v, F and κ are positive constants. For a ratio of diffusion coefficients $K_u/K_v > 1$, the model is known to generate different mechanisms of pattern formation depending on the values of the feed, F, and depletion, κ, rates. Here we select $K_u = 2 \times 10^{-5}$, $K_u/K_v = 2$, $F = 0.03$, and vary κ in a range in which the standard diffusion model is known to exhibit interesting dynamics [34]. The domain of interest is taken to be $[0, 1]^2$, discretised using $N = 400$ points in each spatial coordinate. Initially, the entire system was placed in the trivial state $(u, v) = (1, 0)$, and a 32×32 mesh point area located symmetrically about the centre of the grid was perturbed to $(u, v) = (1/2, 1/4)$. The initial disturbance then propagates outward from the central square until the entire grid is affected by the initial perturbation.

Figure 7 summarizes the effects of fractional diffusion in the Gray–Scott model. For $\kappa = 0.055$ (Fig. 7a), the model with standard diffusion ($\alpha = 2$) is known to organize in a steady state field of negative solitons. A reduction in the fractional order

(a) $\kappa = 0.055$

(b) $\kappa = 0.061$

(c) $\kappa = 0.063$
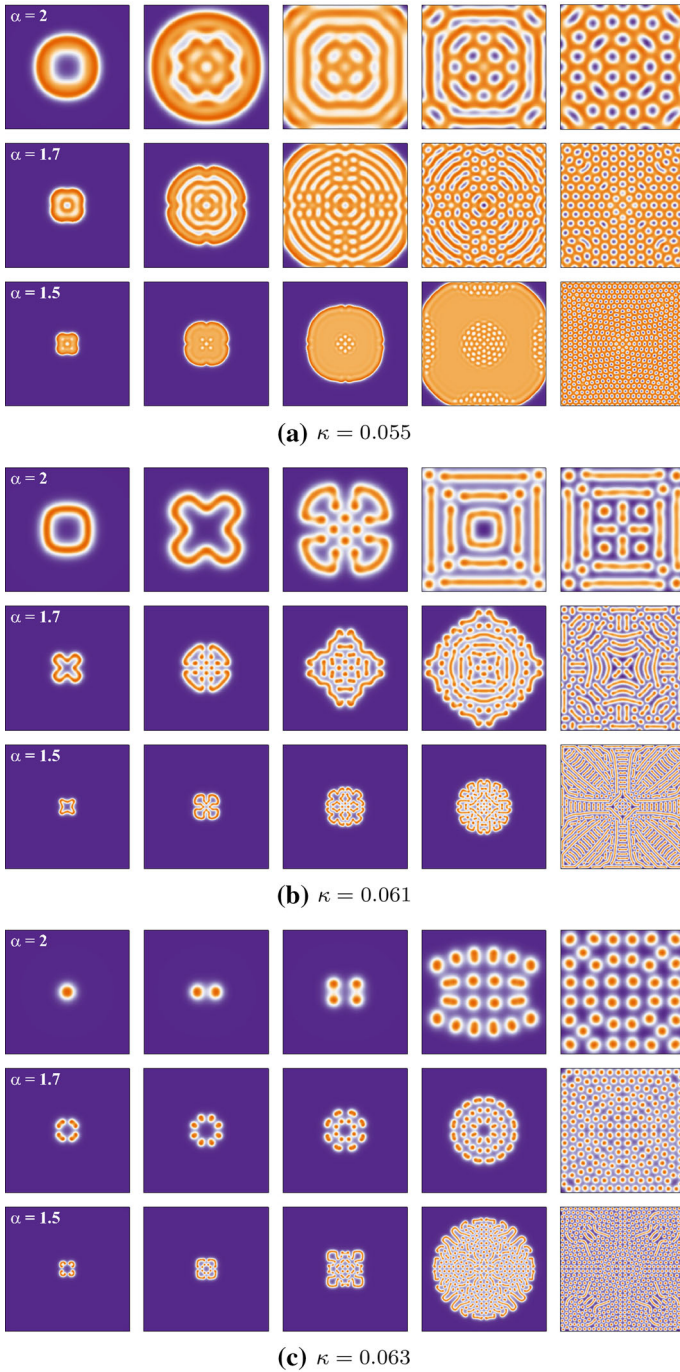
Fig. 7 Pattern formation in the Gray–Scott model for different values of parameter κ and fractional power α

of the diffusive process ($\alpha = 1.7$) produces a decrease in the velocity of propagation of the initial perturbation, and a much finer granulation in the size of the structures of the final steady state field. For smaller values of the fractional power ($\alpha = 1.5$), a new process of nucleation of structures in the centre and in the boundaries of the domain is observed, that then grow outward until the entire domain reaches its final steady state configuration.

For $\kappa = 0.061$ (Fig. 7b), the original model produces a wavefront propagation partially driven by curvature, and a final steady state pattern showing the presence of filaments. The curvature driven mechanisms are increased by the diffusive effects of the fractional Laplacian operator, yielding a final field formed by much thiner filaments, and steady state patterns totally different to those generated by standard diffusion.

Finally, the Gray–Scott model exhibits mitosis for $\kappa = 0.063$ under conditions of normal diffusion (Fig. 7c). However, the replication pattern is completely altered when the fractional order of the model is decreased, as shown in this Figure for $\alpha = 1.7$. In fact, further reductions of the fractional power, as shown for $\alpha = 1.5$, produce dynamical states where solitons and filaments may coexist, the latter slowing self-dividing into the former until the whole domain is filled by a soliton-like pattern.

3.4 Gray–Scott model: patterns in three dimensional space

Numerical simulation of the Gray–Scott model in three spatial dimensions represents an even more interesting scenario where more exotic patterns may arise. For the parameter regime where wavefront motion is partially driven by curvature ($\kappa = 0.061$), and for two different α, Fig. 8 illustrates the three dimensional propagation of the initial perturbation before the interaction of the solution with the domain boundaries. As can be clearly appreciated, the smooth growing of lobes in the presence of normal diffusion (Fig. 8a) is replaced by more intriguing patterns in the fractional diffusion case (Fig. 8b). For improvement of visualization results, the domain size is $[0, 1]^3$ in Fig. 8a, and $[0.25, 0.75]^3$ in Fig. 8b. Note that, for a spatial discretisation of $N = 256$ points in each space dimension, the numerical solution of this problem using finite differences would involve the solution of a linear system of $4N^6 \approx 10^{15}$ equations per time step, which falls outside reasonable computational limits even by using matrix transfer techniques to keep the sparsity of the standard Laplacian discretisation [11,43]. On the other hand, our Fourier implementation yields the solution of two fully diagonal systems of N^3 unknowns, which can be directly updated without requiring the solution of any linear system.

4 Conclusions

In this paper, Fourier spectral methods have been introduced as an attractive and easy-to-code alternative for the integration of fractional-in-space reaction-diffusion equations. These methods offer several advantages over traditional alternatives. Since the operator is non-local, the benefits of using a basis with locally supported elements are destroyed. Hence, the use of an orthogonal, with respect to the opera-

(a) $\alpha = 2$

(b) $\alpha = 1.5$
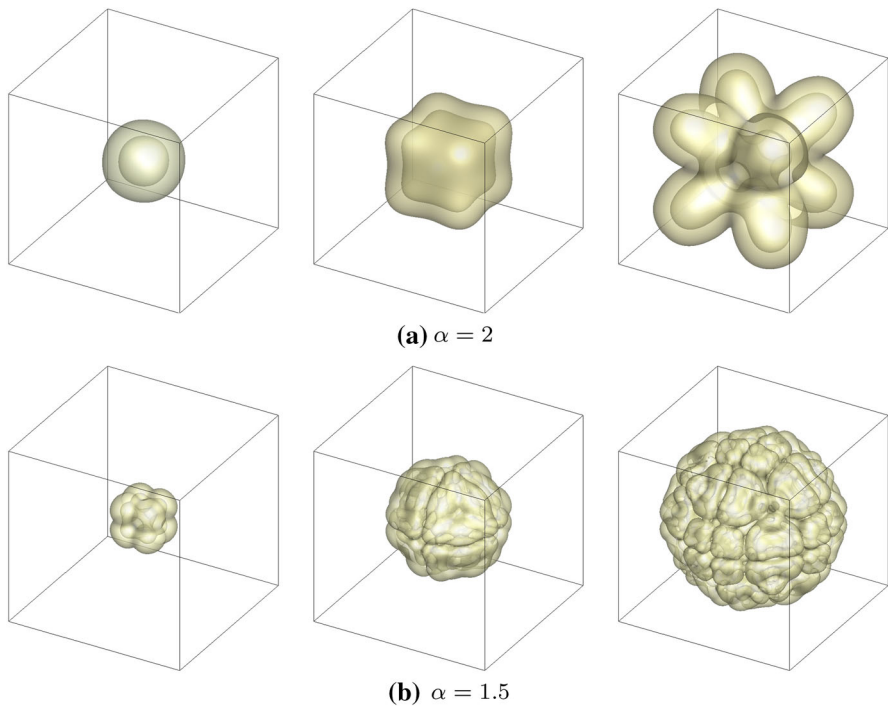
Fig. 8 Isosurfaces $u = 0.65$ for the Gray–Scott model for $\kappa = 0.061$

tor, non-local basis is preferable and will give rise to a fully diagonal representation of the fractional operator, thus avoiding the solution of large systems of equations or the use of matrix transfer techniques. In terms of accuracy and efficiency, Fourier methods have been proven to be not only advantageous relative to memory requirements (number of discretisation points) when compared to low-order schemes, but also computationally efficient in execution times. Furthermore, the use of established discrete fast Fourier transforms ensures efficiency, makes immediate the implementation of appropriate boundary conditions, and allows the extension of the stencil to two and three dimensions in a completely straightforward manner.

Simulation results of the fractional-in-space Allen–Cahn, FitzHugh–Nagumo and in particular Gray–Scott models show that such systems can exhibit dramatically different dynamics to standard diffusion, and as such represent a powerful modelling approach for understanding the many aspects of heterogeneity in excitable media. The efficiency of the Fourier spectral methods developed in this paper allows the simulation of these systems with a level of spatial resolution unreported to date in fractional calculus computations in two and three dimensions.

However, and as expected for Fourier spectral methods, a larger number of discretisation points is required to significantly reduce the approximation error in the presence of steep numerical gradients (see Fig. 3). This can be particularly relevant for slower diffusion rates, such as those in the range $0 < \alpha \leq 1$. In this regard, the

results presented in [46], where the Fourier coefficients of a non-local peridynamic continuum model were shown to converge to those of the original Laplace operator, may help to improve convergence rates at these super-diffusive regimes.

Recent work in combining spectral methods with domain embedding techniques has allowed the extension of spectral methods to irregular domains [7,9,10,26,36]. The use of these techniques may constitute a suitable approach for extending our results in the fractional-in-space setting to irregular shape geometries. Finally, spatial adaptivity can be incorporated in spectral methods by means of spatial mappings [2] or the so-called moving mesh techniques, also known as r-adaptivity [13,31]. All these points, including the existence of variable coefficients in fractional-in-space reaction diffusion equations, constitute current lines of our future work.

References

1. Adams, E.E., Gelhar, L.W.: Field study of dispersion in a heterogeneous aquifer: 2. Spatial moment analysis. Water Resour. Res. **28**, 3293–3307 (1992)
2. Alexandrescu, A., Bueno-Orovio, A., Salgueiro, J.R., Pérez-García, V.M.: Mapped Chebyshev pseudospectral method to study multiple scale phenomena. Comput. Phys. Commun. **180**, 912–919 (2009)
3. Allen, S.M., Cahn, J.W.: A microscopic theory for antiphase boundary motion and its application to antiphase domain coarsening. Acta Metall. Mater. **27**, 1085–1095 (1979)
4. Becker-Kern, P., Meerschaert, M.M., Scheffler, H.P.: Limit theorem for continuous time random walks with two time scales. J. App. Prob. **41**, 455–466 (2004)
5. Benson, D.A., Wheatcraft, S., Meerschaert, M.M.: Application of a fractional advection-dispersion equation. Water Resour. Res. **36**, 1403–1412 (2000)
6. Briggs, W.L., Henson, V.E.: The DFT: an owner's manual for the discrete Fourier transform. SIAM, Philadelphia (2000)
7. Bueno-Orovio, A.: Fourier embedded domain methods: periodic and C^∞ extension of a function defined on an irregular region to a rectangle via convolution with Gaussian kernels. App. Math. Comp. **183**, 813–818 (2006)
8. Bueno-Orovio, A., Cherry, E.M., Fenton, F.H.: Minimal model for human ventricular action potentials in tissue. J. Theor. Biol. **253**, 554–560 (2008)
9. Bueno-Orovio, A., Pérez-García, V.M.: Spectral smoothed boundary methods: the role of external boundary conditions. Numer. Meth. Part. Differ. Equ. **22**, 435–448 (2006)
10. Bueno-Orovio, A., Pérez-García, V.M., Fenton, F.H.: Spectral methods for partial differential equations in irregular domains: the spectral smoothed boundary method. SIAM J. Sci. Comput. **28**, 886–900 (2006)
11. Burrage, K., Hale, N., Kay, D.: An efficient implicit FEM scheme for fractional-in-space reaction-diffusion equations. SIAM J. Sci. Comput. **34**, A2145–A2172 (2012)
12. Engler, H.: On the speed of spread for fractional reaction-diffusion equations. Int. J. Diff. Eqn. **315**, 421 (2010)
13. Feng, W.M., Yu, P., Hu, S.Y., Liu, Z.K., Du, Q., Chen, L.Q.: Spectral implementation of an adaptive moving mesh method for phase-field equations. J. Comput. Phys. **220**, 498–510 (2006)
14. FitzHugh, R.: Impulses and physiological states in theoretical models of nerve membranes. Biophys. J. **1**, 445–466 (1961)
15. Gray, P., Scott, S.K.: Autocatalytic reactions in the isothermal, continuous stirred tank reactor. Isolas and other forms of multistability. Chem. Eng. Sci. **38**, 29–43 (1983)
16. Gray, P., Scott, S.K.: Sustained oscillations and other exotic patterns of behavior in isothermal reactions. J. Phys. Chem. **89**, 22–32 (1985)
17. Hanert, E.: A comparison of three Eulerian numerical methods for fractional-order transport models. Environ. Fluid Mech. **10**, 7–20 (2010)
18. Ilić, M., Liu, F., Turner, I., Anh, V.: Numerical approximation of a fractional-in-space diffusion equation. I. Frac. Calc. App. Anal. **8**, 323–341 (2005)

19. Ilić, M., Turner, I.W.: Approximating functions of a large sparse positive definite matrix using a spectral splitting method. ANZIAM J. **46**, C472–C487 (2005)
20. Khader, M.M.: On the numerical solutions for the fractional diffusion equation. Commun. Nonlinear Sci. Numer. Simulat. **16**, 2535–2542 (2010)
21. Khader, M.M., Sweilam, N.H.: Approximate solutions for the fractional advection-dispersion equation using Legendre pseudo-spectral method. Comp. Appl. Math. doi:10.1007/s40314-013-0091-x
22. Lefèvre, J., Mangin, J.F.: A reaction-diffusion model of human brain development. PLoS Comput. Biol. **6**, e1000749 (2010)
23. Li, X., Xu, C.: A space-time spectral method for the time fractional diffusion equation. SIAM J. Numer. Anal. **47**, 2108–2131 (2009)
24. Li, X., Xu, C.: Existence and uniqueness of the weak solution of the space-time fractional diffusion equation and a spectral method approximation. Commun. Comput. Phys. **8**, 1016–1051 (2010)
25. Liu, F., Zhuang, P., Anh, V., Turner, I., Burrage, K.: Stability and convergence of the finite difference method for the space-time fractional advection-diffusion equation. App. Math. Comp. **191**, 12–20 (2007)
26. Lui, S.H.: Spectral domain embedding for elliptic PDEs in complex domains. J. Comput. Appl. Math. **225**, 541–557 (2009)
27. Magin, R.L., Abdullah, O., Baleanu, D., Zhou, X.J.: Anomalous diffusion expressed through fractional order differential operators in the Bloch-Torrey equation. J. Magn. Reson. **190**, 255–270 (2008)
28. Meerschaert, M.M., Benson, D.A., Wheatcraft, S.W.: Subordinated advection-dispersion equation for contaminant transport. Water Resour. Res. **37**, 1543–1550 (2001)
29. Meerschaert, M.M., Tadjeran, C.: Finite difference approximations for two-sided space-fractional partial differential equations. App. Num. Math. **56**, 80–90 (2006)
30. Metzler, R., Klafter, J.: The random walk's guide to anomalous diffusion: a fractional dynamics approach. Phys. Rep. **339**, 1–77 (2000)
31. Mulholland, L.S., Huang, W.Z., Sloan, D.M.: Pseudospectral solution of near-singular problems using numerical coordinate transformations based on adaptivity. SIAM J. Sci. Comput. **19**, 1261–1289 (1998)
32. Nagumo, J., Animoto, S., Yoshizawa, S.: An active pulse transmission line simulating nerve axon. Proc. Inst. Radio Eng. **50**, 2061–2070 (1962)
33. Pang, H.K., Sun, H.W.: Multigrid method for fractional diffusion. J. Comp. Phys. **231**, 693–703 (2012)
34. Pearson, J.E.: Complex patterns in a simple system. Science **261**, 189–192 (1993)
35. Roop, J.: Computational aspects of FEM approximations of fractional advection dispersion equations on bounded domains on R^2. J. Comp. Appl. Math. **193**, 243–268 (2005)
36. Sabetghadam, F., Sharafatmandjoor, S., Norouzi, F.: Fourier spectral embedded boundary solution of the Poisson's and Laplace equations with Dirichlet boundary conditions. J. Comput. Phys. **228**, 55–74 (2009)
37. Scalas, E., Gorenflo, R., Mainardi, F.: Fractional calculus and continuous time finance. Phys. A **284**, 376–384 (2000)
38. Trefethen, L.N.: Spectral methods in Matlab. SIAM, Philadelphia (2000)
39. Turner, I., Ilić, M., Perr, P.: The use of fractional-in-space diffusion equations for describing microscale diffusion in porous media. In: 11th International Drying Conference, Magdeburg, Germany (2010)
40. Wang, H., Wang, K.: An $O(N \log^2 N)$ alternating-direction finite difference method for two-dimensional fractional diffusion equations. J. Comput. Phys. **230**, 7830–7839 (2011)
41. Wang, H., Wang, K., Sircar, T.: A direct $O(N \log^2 N)$ finite difference method for fractional diffusion equations. J. Comput. Phys. **229**, 8095–8104 (2010)
42. Yang, Q., Liu, F., Turner, I.: Numerical methods for fractional partial differential equations with Riesz space fractional derivatives. App. Num. Mod. **34**, 200–218 (2010)
43. Yang, Q., Turner, I., Liu, F., Ilić, M.: Novel numerical methods for solving the time-space fractional diffusion equation in 2D. SIAM J. Sci. Comp. **33**, 1159–1180 (2011)
44. Zayernouri, M., Karniadakis, G.E.: Fractional spectral collocation method. SIAM J. Sci. Comput. **36**, A40–A62 (2014)
45. Zhang, Y., Benson, D.A., Reeves, D.M.: Time and space nonlocalities underlying fractional-derivative models: distinction and literature review of field applications. Adv. Water Res. **32**, 561–581 (2009)
46. Zhou, K., Du, Q.: Mathematical and numerical analysis of linear peridynamic models with nonlocal boundary conditions. SIAM J. Numer. Anal. **48**, 1759–1780 (2010)